Stress-Modulated Magnetoreflectance for the Direct Transitions $\Gamma_{25'}^{3/2} \rightarrow \Gamma_2$, and $\Gamma_{25'}^{1/2} \rightarrow \Gamma_2$, in Germanium

R. L. Aggarwal

Francis Bitter National Magnet Laboratory, Massachusetts Institute of Technology, Cambridge, Massachusetts* 02139

(Received 17 September 1969)

We have measured the stress-modulated magnetoreflectance in germanium at ~ 30 °K over the energy range 0.9–1.3 eV with magnetic fields up to 85 kG applied along a [110] direction. The measurements were made in the Faraday configuration with right and left circularly polarized light. The structure in piezoreflectance observed at zero magnetic field is correlated with transitions from the $J=\frac{3}{2}$ valence-band edge ($\Gamma_{25'}^{3/2}=\Gamma_8^+$) and the spin-orbit split-off valence-band edge ($\Gamma_{25'}^{1/2}=\Gamma_7^+$) to the conduction-band edge ($\Gamma_{2'}=\Gamma_7^-$) at the center of the Brillouin zone. The structure in the magnetopiezoreflectance spectra is analyzed in terms of interband transitions between Landau levels for the valence and conduction bands. Considering the split-off valence-to-conduction-band transitions, we obtain the reduced mass for these transitions, $m_r \equiv m_c m_{so}/(m_{so}-m_c) = (27.2 \pm 0.3) \times 10^{-3} m$, the sum of the g factors $g_c + g_{so} = -13 \pm 3$, and the spin-orbit splitting $\Delta = 0.296 \pm 0.002$ eV. The light- and heavy-mass valence-to-conduction-band transitions have been analyzed using the coupled-band scheme of Pidgeon and Brown in which the valence bands are treated together with the conduction band. With the valence-band parameters of Luttinger $\gamma_1^L = 13.38$, $\gamma_2^L = 4.30$, $\gamma_3^L = 5.68$, and $\kappa^L = 3.41$ as determined by Hensel and Suzuki from combined resonances in uniaxially stressed p-type germanium, the best fit to the experimental data for the light- and heavy-mass transitions is obtained with the following parameters: the interaction energy between the conduction and valence bands $E_p = 26.8 \pm 0.4$ eV, the parameter $F = (-1.1 \pm 0.2)(\hbar^2/m)$ which represents the conduction-band interaction with the other bands. These parameters give $m_c = (0.0380 \pm 0.0005)m$, and $g_c = -3.0 \pm 0.2$, which are in excellent agreement with those obtained from the conventional magnetoabsorption measurements. With these values of m_c and g_c, we deduce from our results for the split-off transitions $m_{so} = -(0.095 \pm 0.007)m$ and $g_{so} = -10 \pm 3$.

I. INTRODUCTION

Recently, several workers have used modulation techniques such as electroreflectance, piezoreflectance, and thermoreflectance to obtain enhanced sensitivity for the observation of interband transitions in solids. Since the initial observation of oscillatory magnetoabsorption for the direct transition in germanium by Zwerdling *et al.*,[1] Vrehen and Lax[2] applied the method of electric field modulation to magnetoabsorption experiments for the direct transition in germanium. Absorption measurements with transmitted radiation are, however, limited to photon energies close to the energy gap, since even extremely thin samples which are only a few microns thick become opaque at the higher energies. We have chosen to use the piezoreflectance technique of Engeler *et al.*[3] to study the magnetoabsorption for the direct transition in germanium. The magnetopiezoreflectance spectra observed at room temperature have been reported previously.[4] Similar results were obtained with magnetoelectroreflectance at 300 °K.[5]

In this paper, we present the results of magnetopiezoreflectance measurements in germanium at liquid-helium temperatures. The spectra for the valence-to-conduction-band transitions at $\vec{k}=0$ are described in Sec. IV. The experimental results are interpreted in terms of the Pidgeon and Brown[6] analysis outlined in Sec. III for the energy levels of the valence and conduction bands in a magnetic field. In the solution of the two 4×4 matrices for the magnetic energy levels, we have included terms due to static stress which is introduced in the specimen at low temperatures on account of the differential contraction of the specimen relative to the transducer used for stress modulation.

II. EXPERIMENTAL PROCEDURE

A schematic of the apparatus used for the magnetopiezoreflectance measurements is shown in Fig. 1. The setup is very similar to that described previously for room-temperature experiments.[4] For the low-temperature measurements, the piezoelectric transducer of lead-zirconate-titanate used for applying modulating stress to the specimen was held in contact with the cold finger of a cryostat. With liquid helium as the coolant the sample temperature was measured to be ~ 30 °K. The specimens were mounted on the transducer with vacuum grease which freezes at low temperatures to provide a rigid bond between the sample and the transducer. An important advantage of using grease as a cement is that it minimizes the chances of introducing *inhomogeneous* strains in the sample during

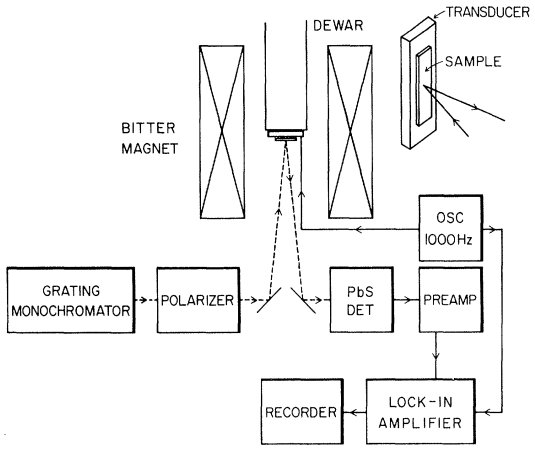

FIG. 1. Block diagram of the experimental setup for magnetopiezoreflectance measurements.

the process of cooling. In addition it may be possible to vary the magnitude of the *homogeneous* static strain which results from the differential contraction of the sample and the transducer by a proper selection of the grease, since all greases do not freeze at the same temperature.[7]

Single-crystal samples of high-purity germanium ($\rho \simeq 40\ \Omega$ cm at 300 °K) were used in the present measurements. The samples were x-ray oriented, sliced, and lapped to a thickness of ~0.4 mm. After lapping, the specimens were etched for 1–2 min in a solution of HNO_3 and HF in the ratio of 3:1.

The magnetopiezoreflectance spectra were recorded with samples in the Faraday configuration for magnetic fields up to 90 kG. A 1.08-μ quarter-wave plate along with a Polaroid HR linear polarizer[8] was employed for obtaining circularly polarized radiation. It may be pointed out, however, that this arrangement does not provide complete circular polarization over the whole range of measurements (0.85 – 1.3 eV) reported in this paper.

III. THEORETICAL

A. Magnetic Energy Levels in Strained Germanium

For strain-free samples, the best theoretical analysis available for the calculation of the magnetic energy levels in the conduction and valence bands at the Γ point is due to Pidgeon and Brown[6] who treat the conduction band together with the degenerate valence-band set. The effective-mass Hamiltonian is then an 8×8 matrix $\underline{D}$ which for the magnetic field $\vec{H}$ in the $(1\bar{1}0)$ plane is written as the sum of two parts,

$$\underline{D} = \underline{D}_0 + \underline{D}_1 \ , \tag{1}$$

where $\underline{D}_1$ is the small part arising from the anisotropy of the valence band. The large part $\underline{D}_0$ also contains part of the anisotropy and can be solved exactly. For $k_H = 0$, corresponding to the singularities in the density of states which give rise to peaks in the absorption spectra, $\underline{D}_0$ decouples into two 4×4 matrices which satisfy the eigenvalue equations in matrix form

$$(\underline{D}_a - \epsilon_a \underline{1}) f_a = 0, \quad (\underline{D}_b - \epsilon_b \underline{1}) f_b = 0 \ , \tag{2}$$

where ϵ_a and ϵ_b are the eigenvalues and the functions f_a and f_b are expressed in terms of the harmonic-oscillator functions φ_n:

$$f_a = \begin{vmatrix} c_1\varphi_n \\ c_3\varphi_{n-1} \\ c_5\varphi_{n+1} \\ c_7\varphi_{n+1} \end{vmatrix}, \quad f_b = \begin{vmatrix} c_2\varphi_n \\ c_6\varphi_{n-1} \\ c_4\varphi_{n+1} \\ c_8\varphi_{n-1} \end{vmatrix}, \tag{3}$$

where c_1, c_2, etc., are the eigenvectors. The complete wave functions are of the form

$$\begin{aligned} \Psi_a(n) &= c_1u_1\varphi_n + c_3u_3\varphi_{n-1} + c_5u_5\varphi_{n+1} + c_7u_7\varphi_{n+1}, \\ \Psi_b(n) &= c_2u_2\varphi_n + c_6u_6\varphi_{n-1} + c_4u_4\varphi_{n+1} + c_8u_8\varphi_{n-1} . \end{aligned} \tag{4}$$

The u_j are linear combinations of the s-like and p-like band-edge Bloch functions

$$\begin{aligned} u_1 &= S\uparrow, & u_2 &= S\downarrow , \\ u_3 &= \frac{1}{\sqrt{2}}(X+iY)\uparrow , & u_4 &= \frac{i}{\sqrt{2}}(X-iY)\downarrow , \\ u_5 &= \frac{1}{\sqrt{6}}[(X-iY)\uparrow + 2Z\downarrow], & u_6 &= \frac{i}{\sqrt{6}}[(X+iY)\downarrow - 2Z\uparrow], \\ u_7 &= \frac{i}{\sqrt{3}}[-(X-iY)\uparrow + Z\downarrow], & u_8 &= \frac{1}{\sqrt{3}}[(X+iY)\downarrow + Z\uparrow], \end{aligned} \tag{5}$$

where $\uparrow$ and $\downarrow$ stand for the spin-up and spin-down functions, respectively, S is the atomic s-like conduction-band function, and X, Y, and Z are the atomic p-like valence-band functions.

1. *Perturbation due to Strain*

The effect of uniaxial stress or of the two-dimensional stress on the energy levels may be obtained by including the stress terms in D_0. Instead of pursuing the general problem, we will consider the particular case applicable in the present experiment, viz., the two-dimensional stress in the (110) plane with the magnetic field applied along the [110] direction. In the $\langle JM_J\rangle$ representation, the strain Hamiltonian for the $J = \frac{3}{2}$ valence-band edge is given by the matrix[9]

$$H_s = \begin{array}{c|cccc|c} & & & & & M_J \\ & \epsilon_1 & \epsilon_2 & 0 & 0 & \frac{3}{2} \\ & \epsilon_2 & -\epsilon_1 & 0 & 0 & -\frac{1}{2} \\ & 0 & 0 & -\epsilon_1 & \epsilon_2 & \frac{1}{2} \\ & 0 & 0 & \epsilon_2 & \epsilon_1 & -\frac{3}{2} \end{array} , \tag{6}$$

where $\epsilon_1 = -\frac{1}{4}(1+\lambda)(b+\sqrt{3}d)S$,
$\epsilon_2 = \frac{3}{4}(1+\lambda)(b-d/\sqrt{3})S$, (7)

with $\lambda = \dfrac{c_{11}+3c_{12}-2c_{44}}{c_{11}+c_{12}+2c_{44}}$, (8)

where b and d are the valence-band deformation potentials; c_{11}, c_{12}, and c_{44} are the elastic constants; and S is the strain in the (110) plane. The splitting of the valence-band edge for a (110) strain is

$$2(\epsilon_1^2+\epsilon_2^2)^{1/2}. \tag{9}$$

The strain can be determined from Eq. (9) using Eq. (7).

The center-of-gravity shift of the valence band with respect to the conduction band is given by

$$\delta\epsilon_g = a(2-\lambda)S, \tag{10}$$

where a is the deformation potential for isotropic dilation and is given by

$$a = -\tfrac{1}{3}(c_{11}+2c_{12})\frac{d\epsilon_g}{dp}, \tag{11}$$

where $d\epsilon_g/dp$ is the pressure coefficient for the energy gap.

Using the values of the deformation potentials $b = 2.6$ eV and $d = 4.7$ eV as measured by Pollak *et al.*,[10] it follows that $|\epsilon_2| \ll |\epsilon_1|$. Thus we may neglect ϵ_2 to render H_S diagonal in the $\langle JM_J\rangle$ representation. If we further neglect the small matrix elements between the valence-band edge and the split-off band,[11] the Hamiltonian for the strained crystal in a magnetic field is obtained by including $\delta\epsilon_g$ and the elements of H_S in the diagonal terms of D_a and D_b matrices. Thus, the determinantal equations for the eigenvalues of the a and b sets for the two-dimensional stress in the (110) plane and the magnetic field along the [110] direction are[12]

$$\begin{vmatrix}
\epsilon_g+\delta\epsilon_g+s(n+1)+(2m/\hbar^2)sF(n+\frac{1}{2})-\epsilon_a & i(\frac{1}{2}snE_p)^{1/2} & i[\frac{1}{6}s(n+1)E_p]^{1/2} & [\frac{1}{3}s(n+1)E_p]^{1/2} \\
-i(\frac{1}{2}snE_p)^{1/2} & -s[(\gamma_1+\gamma')(n-\frac{1}{2})+\frac{3}{2}\kappa]-\epsilon_1-\epsilon_a & -s[3n(n+1)]^{1/2}\gamma'' & -is[6n(n+1)]^{1/2}\gamma'' \\
-i[\frac{1}{6}s(n+1)E_p]^{1/2} & -s[3n(n+1)]^{1/2}\gamma'' & -s[(\gamma_1-\gamma')(n+\frac{3}{2})-\frac{1}{2}\kappa]+\epsilon_1-\epsilon_a & is(2)^{1/2}[\gamma'(n+\frac{3}{2})-\frac{1}{2}(\kappa+1)] \\
[\frac{1}{3}s(n+1)E_p]^{1/2} & is[6n(n+1)]^{1/2}\gamma'' & -is(2)^{1/2}[\gamma'(n+\frac{3}{2})-\frac{1}{2}(\kappa+1)] & -s[\gamma_1(n+\frac{3}{2})-\kappa-\frac{1}{2}]-\Delta-\epsilon_a
\end{vmatrix} = 0 \tag{12}$$

and

$$\begin{vmatrix}
\epsilon_g+\delta\epsilon_g+sn+(2m/\hbar^2)sF(n+\frac{1}{2})-\epsilon_b & i(\frac{1}{6}snE_p)^{1/2} & i[\frac{1}{2}s(n+1)E_p]^{1/2} & (\frac{1}{3}snE_p)^{1/2} \\
-i(\frac{1}{6}snE_p)^{1/2} & -s[(\gamma_1-\gamma')(n-\frac{1}{2})+\frac{1}{2}\kappa]+\epsilon_1-\epsilon_b & -s[3n(n+1)]^{1/2}\gamma'' & is(2)^{1/2}[\gamma'(n-\frac{1}{2})+\frac{1}{2}(\kappa+1)] \\
-i[\frac{1}{2}s(n+1)E_p]^{1/2} & -s[3n(n+1)]^{1/2}\gamma'' & -s[(\gamma_1+\gamma')(n+\frac{3}{2})-\frac{3}{2}\kappa]-\epsilon_1-\epsilon_b & is[6n(n+1)]^{1/2}\gamma'' \\
(\frac{1}{3}snE_p)^{1/2} & -is(2)^{1/2}[\gamma'(n-\frac{1}{2})+\frac{1}{2}(\kappa+1)] & -is[6n(n+1)]^{1/2}\gamma'' & -s[\gamma_1(n-\frac{1}{2})+\kappa+\frac{1}{2}]-\Delta-\epsilon_b
\end{vmatrix} = 0\,. \tag{13}$$

Here $s = \hbar eH/mc$ is equal to the cyclotron energy for a free electron; E_p is the interaction energy between the conduction and valence bands defined as[13]

$$E_p = (2m/\hbar^2)P^2\,; \tag{14}$$

P is the momentum matrix element between the conduction band and the valence band; F represents the interaction of the conduction band with the higher bands.[14] γ_1, γ_2, γ_3, and κ are the valence-band parameters due to the higher-band contributions[6]

$$\gamma_1 = \gamma_1^L - E_p/3\epsilon_g, \quad \gamma_2 = \gamma_2^L - E_p/6\epsilon_g,,$$
$$\gamma_3 = \gamma_3^L - E_p/6\epsilon_g, \quad \kappa = \kappa^L - E_p/6\epsilon_g, \tag{15}$$

where γ_1^L, γ_2^L, γ_3^L, and κ^L are the valence-band

parameters defined by Luttinger. γ' and γ'' are given in terms of γ_2 and γ_3 and the angle θ between the magnetic field and the crystal z axis. Δ is the spin-orbit splitting energy for the valence band.

B. Cyclotron Masses and g Factors

We can obtain expressions for the band-edge masses and g factors from the solutions of Eqs. (12) and (13).

1. *Conduction Band*

The energies of the two lowest Landau levels corresponding to $n=0$ and 1 are given by Eq. (12) for the a series as

$$\epsilon_a^c(0)=(\epsilon_g+\delta\epsilon_g)+s\left[1+\frac{m}{\hbar^2}F+\tfrac{1}{6}E_p\left(\frac{1}{\epsilon_g+\delta\epsilon_g}+\frac{2}{\epsilon_g+\delta\epsilon_g+\Delta}\right)\right], \tag{16}$$

$$\epsilon_a^c(1)=(\epsilon_g+\delta\epsilon_g)+s\left[2+\frac{3m}{\hbar^2}F+\tfrac{1}{6}E_p\left(\frac{5}{\epsilon_g+\delta\epsilon_g}+\frac{4}{\epsilon_g+\delta\epsilon_g+\Delta}\right)\right] \tag{17}$$

in the limit of small magnetic field, i.e., $s\ll\epsilon_g,\Delta$.

Similarly, we obtain from Eq. (13) the energies of the $n=0$ and $n=1$ Landau levels for the b series,

$$\epsilon_b^c(0)=(\epsilon_g+\delta\epsilon_g)+s\left(\frac{m}{\hbar^2}F+\frac{3E_p}{6(\epsilon_g+\delta\epsilon_g)}\right), \tag{18}$$

and

$$\epsilon_b^c(1)=(\epsilon_g+\delta\epsilon_g)+s\left[1+\frac{3m}{\hbar^2}F+\tfrac{1}{6}E_p\left(\frac{7}{\epsilon_g+\delta\epsilon_g}+\frac{2}{\epsilon_g+\delta\epsilon_g+\Delta}\right)\right]. \tag{19}$$

Subtracting Eq. (17) from Eq. (16) [or Eq. (19) from Eq. (18)], we get the conduction-band mass m_c given by

$$\frac{m}{m_c}=1+\frac{2m}{\hbar^2}F+\tfrac{1}{3}E_p\left(\frac{2}{\epsilon_g+\delta\epsilon_g}+\frac{1}{\epsilon_g+\delta\epsilon_g+\Delta}\right). \tag{20}$$

Except for the small term containing F, the above expression for m_c is the same as that of Kane[14] for zero magnetic field. Subtracting Eq. (18) from Eq. (16), we obtain the conduction-band g factor

$$g_c=2\left(1-\frac{E_p}{3(\epsilon_g+\delta\epsilon_g)}\,\frac{\Delta}{(\epsilon_g+\delta\epsilon_g+\Delta)}\right). \tag{21}$$

The above expression for g_c is identical to that deduced by Roth *et al.*[15] It is interesting to note that in the limit $\Delta=0$, $g_c=2$, a value equal to that for the free electron. In the other extreme, when $\Delta\to\infty$,

$$g_c=2[1-\tfrac{1}{3}E_p/(\epsilon_g+\delta\epsilon_g)]\simeq -m/m_c,$$

i.e., the g factor becomes equal to the reciprocal of the effective mass.

2. *Split-Off Band*

The energies of the two lowest Landau levels of the a series corresponding to $n=-1$ and 0 in the Pidgeon-Brown (PB) notation are obtained from the solutions of Eq. (12) for small magnetic fields so that $s\ll\epsilon_g$, Δ. In that case

$$\epsilon_a^{so}(-1)=-\Delta-s(\tfrac{1}{2}\gamma_1-\kappa-\tfrac{1}{2}) \tag{22}$$

and

$$\epsilon_a^{so}(0)=-\Delta-s\left((\tfrac{2}{3}\gamma_1-\kappa-\tfrac{1}{2})+\frac{E_pE_p}{3(\epsilon_g+\delta\epsilon_g+\Delta)}\right). \tag{23}$$

Similarly, we obtain the following expressions from the solutions of Eq. (13) for the two lowest Landau levels of the b series corresponding to $n=1$ and 2 in the PB notation:

$$\epsilon_b^{so}(1)=-\Delta-s\left((\tfrac{1}{2}\gamma_1+\kappa+\tfrac{1}{2})+\frac{E_p}{3(\epsilon_g+\delta\epsilon_g)}\right), \tag{24}$$

$$\epsilon_b^{so}(2)=-\Delta-s\left((\tfrac{3}{2}\gamma_1+\kappa+\tfrac{1}{2})+\frac{2E_p}{3(\epsilon_g+\delta\epsilon_g+\Delta)}\right). \tag{25}$$

From Eqs. (22) and (23) [or Eqs. (24) and (25)], we obtain the split-off band mass as given by

$$m/m_{so}=-[\gamma_1+E_p/3(\epsilon_g+\delta\epsilon_g+\Delta)]. \tag{26a}$$

In terms of Luttinger parameters, it becomes

$$\frac{m}{m_{so}}=-\left(\gamma_1{}^L-\frac{E_p}{3(\epsilon_g+\delta\epsilon_g)}\,\frac{\Delta}{(\epsilon_g+\delta\epsilon_g+\Delta)}\right). \tag{26b}$$

In the case of weak spin-orbit coupling, the above equation will be reduced to $m/m_{so}=-\gamma_1{}^L$, in agreement with the mass appearing in Luttinger's equation (89) for the Landau-level energies of the split-off band.[16]

Subtracting Eq. (22) from Eq. (24), we obtain

$$g_{so}=-2[2\kappa+1+E_p/3(\epsilon_g+\delta\epsilon_g)], \tag{27a}$$

which in terms of the Luttinger parameters becomes

$$g_{so}=-2\left(2\kappa^L+1-\frac{E_p}{3(\epsilon_g+\delta\epsilon_g)}\,\frac{\Delta}{(\epsilon_g+\delta\epsilon_g+\Delta)}\right). \tag{27b}$$

For the weak spin-orbit coupling, Eq. (27b) will simplify to

$$g_{so}=-2[2\kappa^L+1]\quad\text{for }\Delta\ll\epsilon_g. \tag{28}$$

Using Eq. (9b) of Luttinger in Ref. 16, one obtains a g factor of $\frac{1}{3}(2Km-1)=-(2\kappa^L+1)$. Therefore, Luttinger's value is in error by a factor of 2 introduced in transforming from the $\langle L, S\rangle$ representation to the $\langle JM_J\rangle$ representation for the $J=\frac{1}{2}$ band. Our result agrees with that deduced from Eq. (13) of Evtuhov's paper.[17] It should also be mentioned that an additional typographical error in Eq. (89) of Luttinger[16] led Burstein *et al.*[18] to predict the

large value of +54 for the g factor of the split-off band in germanium instead of −15 obtained from Eq. (28) for weak spin-orbit coupling with $\kappa^L = 3.23$.[15] The incorrect sign for the g factor of Burstein *et al.*[18] was the result of their misinterpretation of the sign of Luttinger's antisymmetric constant K. In the 3×3 equations (B9) and (B10) of Roth *et al.*,[15] the g-factor contribution is missing in the diagonal term for the split-off band for no apparent reason.

Another interesting quantity is the sum of the g factors for the conduction and split-off bands. This is simply obtained by adding Eqs. (21) and (27b) as

$$g_c + g_{so} = -4\kappa^L. \tag{29}$$

This relationship is valid for weak as well as strong spin-orbit coupling. As we will see later, $g_c + g_{so}$ and consequently κ^L is directly determined from the difference in energy for the split-off-to-conduction-band transitions observed in a magnetic field with left and right circularly polarized light propagating along the direction of the magnetic field.

3. *Light and Heavy Valence Bands*

Unlike the Landau levels for the conduction band and the split-off valence bands (neglecting nonparabolic effects), the Landau levels of the light and heavy valence bands at the zone center are not uniformly spaced in energy. This anomalous behavior is most pronounced for low quantum numbers. Therefore, it is meaningless to talk about cyclotron masses and g factors for these bands in the region of so-called "quantum effects." In the classical limit of large n, and small magnetic fields, Eq. (12) yields the following expressions for the light and heavy levels of the a series:

$$\epsilon_a^l/s = n\{\gamma_1^L + [(\gamma'^L)^2 + 3(\gamma''^L)^2]^{1/2}\} - \kappa^L$$

and (30)

$$\epsilon_a^h/s = -n\{\gamma_1^L - [(\gamma'^L)^2 + 3(\gamma''^L)^2]^{1/2}\} - (\gamma_1^L - 2\bar{\gamma}^L), \tag{31}$$

where $\bar{\gamma}^L = \frac{1}{2}(\gamma'^L + \gamma''^L)$.

Similarly we obtain from Eq. (13) for the b series

$$\epsilon_b^l/s = -\{\gamma_1^L + [(\gamma'^L)^2 + 3(\gamma''^L)^2]^{1/2}\} - (\gamma_1^L + 2\bar{\gamma}^L - \kappa^L) \tag{32}$$

and

$$\epsilon_b^h/s = -n\{\gamma_1^L - [(\gamma'^L)^2 + 3(\gamma''^L)^2]^{1/2}\}. \tag{33}$$

Using Eqs. (30) and (31) or (32) and (33), the light and heavy valence-band masses are given by

$$-m/m_l = \gamma_1^L + [(\gamma'^L)^2 + 3(\gamma''^L)^2]^{1/2}, \tag{34}$$

$$-m/m_h = \gamma_1^L - [(\gamma'^L)^2 + 3(\gamma''^L)^2]^{1/2}. \tag{35}$$

Subtracting Eq. (32) from Eq. (31), one obtains for the light-hole g factor

$$g_l = 2(\gamma_1^L + 2\bar{\gamma}^L - 2\kappa^L). \tag{36a}$$

The g factor may be written in terms of m_l,

$$g_l = 2(m/m_l - 2\kappa^L). \tag{36b}$$

Similarly, Eqs. (31) and (33) give the heavy-hole g factor

$$g_h = 2(\gamma_1^L - 2\bar{\gamma}^L) \quad \text{or} \quad g_h = 2m/m_h. \tag{37}$$

We have obtained Eqs. (30)–(37) in the approximation for small magnetic fields, and large n. For infinitesimally small magnetic field, the cyclotron mass for Landau levels with $n \geq 4$ in the PB notation is given by Eqs. (34) and (35) with an error of 1% or less. The fractional error in mass due to finite magnetic fields may be estimated from the following approximate equation:

$$\Delta m^*/m^* \simeq \tfrac{1}{25} nH \text{ (kG)} \times 10^{-2}$$

for the light-mass series. For example, there will be an error of 1.6% for the $n=4$ level at $H=10$ kG. There will be an error of 16% for the same level at $H=100$ kG. This shows that the decoupled scheme in which the interaction of the light and heavy bands with the conduction band is neglected is not valid for the high magnetic fields used in this experiment.

C. Selection Rules and Relative Intensities for Interband Transitions

Using the zeroth-order wave functions $\Psi^I(n)$ and $\Psi^F(n')$ for the initial and final states, respectively, the matrix element for dipole transitions is given by

$$\langle \Psi^F(n') | \vec{\pi}\cdot\vec{\epsilon} | \Psi^I(n) \rangle = \sum_{jj'} (\vec{\pi}_{jj'}\cdot\vec{\epsilon}) \langle f_{j'}(n') | f_j(n) \rangle + \sum_{jj'} \vec{\epsilon}\cdot \langle f_{j'}(n') | \vec{\pi}_{jj'} | f_j(n) \rangle \delta_{jj'}, \tag{38}$$

where $\vec{\pi}_{jj'}$ is the momentum matrix element between the bands j and j' at $\vec{k}=0$. The first term on the right-hand side of Eq. (38) gives the allowed transitions at $\vec{k}=0$. The second term which is small gives the forbidden transitions at $\vec{k}=0$. The latter transitions are analogous to those observed in cyclotron resonance. For the allowed valence-to-conduction-band transitions, $\langle f_{j'}(n') | f_j(n) \rangle$ vanishes unless $n' = n \pm 1$. This selection rule of $\Delta n = \pm 1$ corresponds to the selection rules $\Delta n = 0, -2$ derived by Roth *et al.*[15] The apparent difference in these selection rules is only artificial. This is due to the

fact that in the coupled-band scheme, we obtain a set of envelope functions f_j's different from those of the decoupled scheme used by Roth *et al.*[15] We hope that this change in notation will not cause confusion since the n quantum number for the conduction-band levels is the same in both cases. In addition to the selection rule for Δn, the change in total angular momentum ΔM_J must be 0 or ± 1. In the Voigt configuration in which light propagates along a direction normal to the applied magnetic field $\Delta M_J = 0$ for $\vec{E} \| \vec{H}$ and $\Delta M_J = \pm 1$ for $\vec{E} \perp \vec{H}$. In the Faraday configuration where light propagates parallel to the magnetic field, only transitions corresponding to $\Delta M_J = \pm 1$ are allowed with $\Delta M_J = +1$ for left circularly polarized (LCP) radiation and $\Delta M_J = -1$ for the right circularly polarized (RCP) radiation.

The relative intensities for the allowed transitions are obtained in the same manner as used by Roth *et al.*[15] for the decoupled bands. However, for the amplitudes of the harmonic-oscillator functions, we have used the values obtained from the solution of the coupled-band scheme.

IV. EXPERIMENTAL RESULTS AND DISCUSSIONS

A. Piezoreflectance Spectrum Observed for Zero Magnetic Field

A plot of piezoreflectance $(1/R)\Delta R/\Delta S$ versus photon energy for the direct transitions is shown in Fig. 2. The two direct edges labeled D_1 and D_2 (not to be confused with D matrices in Sec. III A) are, respectively, due to transitions $\Gamma_{25'}^{3/2} \rightarrow \Gamma_{2'}$ and $\Gamma_{25'}^{1/2} \rightarrow \Gamma_{2'}$. In the spectral region of the D_1 edge, the spectrum shown in Fig. 2 exhibits a broad minimum at 0.883 eV, and two sharp minima at 0.893 and 0.896 eV, respectively. An analysis of the line shapes for the piezoreflectance spectra is essential for a complete understanding of the above features exhibited by the observed spectra. Since we have not carried out a study of the line-shape analysis, we will assume for the sake of convenience that the transition energies are given by the positions of piezoreflectance minima. Our only justification for this approach is that in the analysis of the magnetopiezoreflectance spectra which is of primary interest for this paper, use of either minima, maxima, or inflection points yields the same zero-field energy gap on extrapolation as shown by Mavroides.[19] He has also shown, however, that the extrapolated point for $H = 0$ coincides with the inflection point on the zero-field piezoreflectance curve. It should be pointed out that the $\Delta R/R$ values of Mavroides *et al.*[5] should be multiplied by -1 in order to make their spectra compatible with that reported by Engeler *et al.*[3] for germanium at room temperature. As a result of this sign difference,

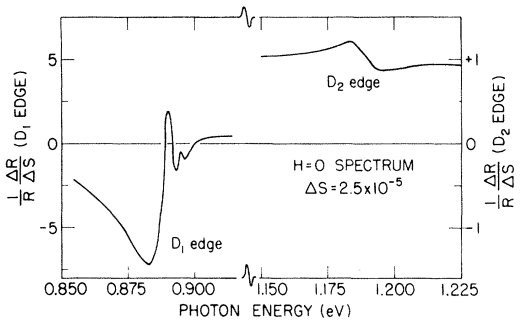

FIG. 2. Piezoreflectance spectrum for the D_1 and D_2 edges in germanium at ~ 30 °K in zero magnetic field.

maxima on the $\Delta R/R$ curves of Mavroides *et al.* correspond to minima in the present paper since we are in agreement with the sign convention of Engeler *et al.*[3]

We interpret the sharp minima at 0.893 and 0.896 eV to correspond to the D_1 edge which is split by the static strain introduced in our samples during the cooling process, as pointed out in Sec. II. The observed splitting of 3 meV represents the strain splitting of the $J = \frac{3}{2}$ valence-band edge. Using Eqs. (7)–(9) and the deformation potentials $b = 2.6$ eV, $d = -4.7$,[10] a splitting of 3 meV corresponds to a strain of 4×10^{-4} for the (110) samples used in these measurements. With $d\epsilon_g/dp = 12 \times 10^{-6}$ eV cm^2/kg,[20] the above value of strain will produce a shift of -5.6 sgn (strain) meV. Since the observed value of 0.894(5) eV for the mean energy gap is higher than the value of 0.8876 eV obtained by Macfarlane *et al.*[21] from conventional absorption measurements with freely mounted samples, it follows that our samples were under compressive stress. In this manner we deduce that the minimum in $\Delta R/R$ for this transition should occur at 0.889 eV in samples with zero static strain. Assuming an exciton binding energy of 1.2 meV, we obtain a value of 0.890 eV for the energy gap on the basis of the minima in $(1/R)\Delta R/\Delta S$. This is in good agreement with Macfarlane's value of 0.8876 eV. If we use the inflection point according to Mavroides's suggestion for the zero-field data, our value for the energy gap is reduced to 0.888(5) eV which is in even better agreement with Macfarlane's result.

In the region of the D_2 edge, a very weak and broad structure is observed with a minimum at 1.194 eV and an inflection point at 1.189 eV. If the hydrostatic deformation potential a for the D_2 edge is assumed to be equal to that for the D_1 edge, we obtain $\epsilon_g + \Delta = 1.183$ eV from the position of the inflection point. This is in good agreement with the observations of Hobden[22] who deduced the existence of the D_2 edge at 1.179 ± 0.005 eV with a half-width of 15 meV from the conventional absorption mea-

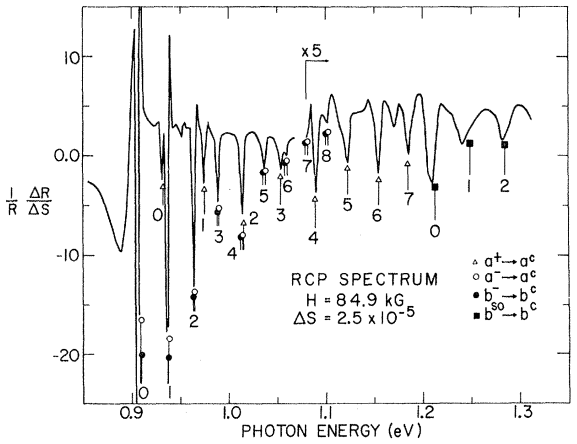

FIG. 3. Magnetopiezoreflectance spectrum for the D_1 and D_2 transitions in germanium at ~30 °K observed in the Faraday configuration with RCP radiation and magnetic field $H=84.9$ kG applied along a ⟨110⟩ direction. The strong minima in $(1/R)\Delta R/\Delta S$ are identified with lines under them which have a characteristic symbol at the top end indicating the type of the transition. The length of a given line is proportional to the oscillator strength of the transition it represents. The positions of the lines are obtained from the solutions of Eqs. (12) and (13) with the following parameters: $\epsilon_g=0.888(5)$ eV, $\Delta=0.296$ eV, $E_p=26.8$ eV, $(m/\hbar^2)F=-1.1$, $\gamma_1^L=13.38$, $\gamma_2^L=4.30$, $\gamma_3^L=5.68$, $\kappa^L=3.41$, $\epsilon_1=-0.0015$ eV, and $\delta\epsilon_g=0.0056$ eV.

surements at 4 °K. From our value of 1.183 eV for $\epsilon_g+\Delta$, we obtain $\Delta=0.295$ eV by subtracting off 0.888 eV for ϵ_g as determined above from the D_1 edge. If we perform a similar analysis using the position of minimum in $\Delta R/R$, we will get $\Delta=0.298$ eV. Both of the above values of Δ are larger than Hobden's[22] value of 0.29 ± 0.005 eV at 4 °K and Seraphin's[23] value of 0.29(2) eV obtained from electroreflectance measurements at room temperature. The above discrepancies between the various measurements are not to be taken seriously in view of the uncertainty in the line-shape analysis for each of the experiments.

B. Piezoreflectance Spectrum Observed in Magnetic Field

In Fig. 3 is shown the magnetopiezoreflectance (MPR) spectrum observed in the Faraday configuration with right circularly polarized radiation and a magnetic field of 84.9 kG applied along a ⟨110⟩ direction. The spectrum for the left circular polarization is shown in Fig. 4. For either polarization of the radiation, the structure in $(1/R)\Delta R/\Delta S$ below 1.2 eV is due to transitions between Landau levels corresponding to the D_1 edge. Above 1.2 eV, the prominent structure appears to be caused by transitions between Landau levels for the split-off band and those for the conduction band.

The $(1/R)\Delta R/\Delta S$ structure shown in Figs. 3 and 4 exhibits the following features: Beginning on the low-energy side, the $(1/R)\Delta R/\Delta S$ structure associated with a given transition consists of a large negative spike which is followed by a smaller positive spike. As we go to higher energies, the size of the positive spikes decreases faster than that of the negative spikes. Above ~1.0 eV only the negative spikes are observed. This is the reason for choosing the minima of $(1/R)\Delta R/\Delta S$ in the analysis of the data in a magnetic field.

In order to obtain band parameters from the MPR spectra, we need to identify the observed transitions with those expected from theory outlined in Sec. III and then compare the experimental and theoretical values for the transition energies. The best fit between theory and experiment for all the transitions will hopefully provide the best set of band-edge parameters.

In view of the complexity of the light and heavy band levels near $\vec{k}=0$, we will discuss the simple case of split-off-to-conduction-band transitions first.

1. *Spin-Orbit Split-Off Valence-to-Conduction-Band Transitions*

Let us assume for the sake of simplicity that the split-off and the conduction bands are parabolic. The Landau-level energies are then given by

$$\epsilon_c(n)=\epsilon_g+\delta\epsilon_g+s\left[(m/m_c)(n+\tfrac{1}{2})\pm\tfrac{1}{4}g_c\right] \tag{39}$$

for the conduction band, and by

$$\epsilon_{so}(n)=-\Delta+s\left[(m/m_{so})(n+\tfrac{1}{2})\pm\tfrac{1}{4}g_{so}\right],$$
$$n=0,\ 1,\ 2,\ \text{etc.}, \tag{40}$$

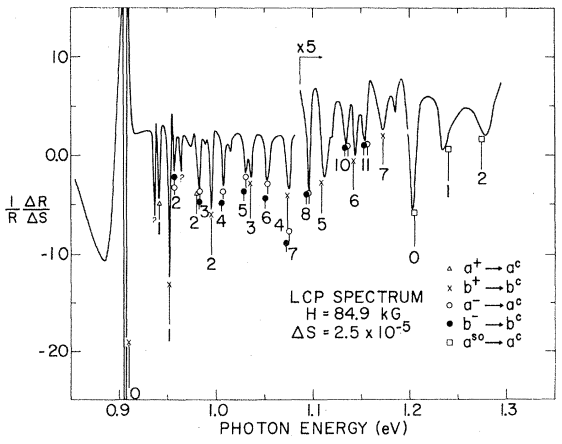

FIG. 4. Magnetopiezoreflectance spectrum for LCP radiation (also see Fig. 3). The minima in $(1/R)\Delta R/\Delta S$ with a question mark occur at the same energy where there is strong structure in the RCP spectrum. These minima in LCP are, therefore, presumably due to incomplete polarization of the circular polarizer.

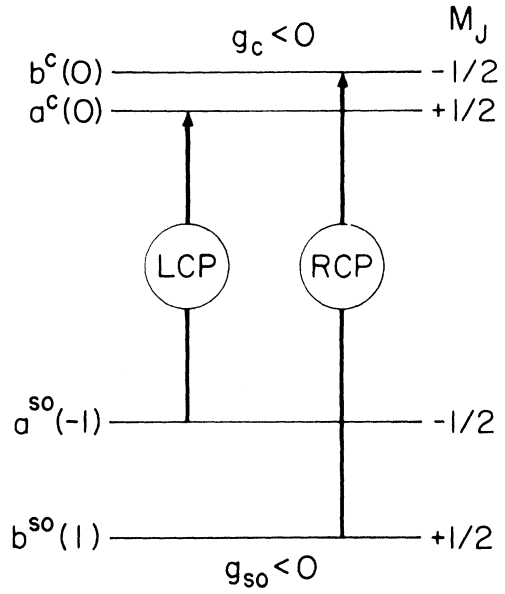

FIG. 5. Schematic of electron transitions involving the first Landau levels of the spin-orbit split-off valence band and the conduction band. The Landau-level labels $a^c(0)$, $b^c(0)$, etc., which appear next to each level on the right-hand side are derived from the coupled-band scheme. $a^{so}(-1)$, for example, denotes the $n=-1$ level of the a series for the split-off band. This corresponds to the first, i.e., $n=0$ level in the decoupled scheme.

for the split-off band. The upper and the lower signs are for $M_J = +\frac{1}{2}$ and $-\frac{1}{2}$, respectively. The interband optical transitions between these levels are allowed in the Faraday configuration for the selection rules $\Delta n = 0$ and $\Delta M_J = \pm 1$. The first Landau levels and the allowed interband transitions are shown schematically in Fig. 5. Photon energies at which these transitions occur are obtained from Eqs. (39) and (40) as

$$\mathcal{E}_{so\to c}(n) = \epsilon_g + \delta\epsilon_g + \Delta + s\left[\left(\frac{m}{m_c} - \frac{m}{m_{so}}\right)(n+\tfrac{1}{2}) \pm \tfrac{1}{4}(g_c + g_{so})\right], \quad (41)$$

where the + and − signs are for the LCP and RCP radiation, respectively. It follows immediately from Eq. (41) that the mean value of the photon energies for a given n is

$$\overline{\mathcal{E}}_{so\to c}(n) = \epsilon_g + \delta\epsilon_g + \Delta + s(m/m_c - m/m_{so})(n+\tfrac{1}{2}). \quad (42)$$

Thus a plot of $\overline{\mathcal{E}}_{so\to c}(n)$ versus $(n+\frac{1}{2})s$ should yield a straight line. The slope of this line will be equal to $1/m_c - 1/m_{so}$ which is the reciprocal of the reduced mass for the conduction and split-off bands in units of the free-electron mass. The intercept of the line on the $\overline{\mathcal{E}}$ axis will be equal to $(\epsilon_g + \delta\epsilon_g + \Delta)$. In Fig. 6 is shown a plot of $\overline{\mathcal{E}}_{so\to c}(n)$ as a function of $(n+\frac{1}{2})s$ for our experimental data for the split-off transitions. From a least-squares fit of the data to a straight line, we obtain $m/m_c - m/m_{so} = 36.8 \pm 0.3$, and $\epsilon_g + \delta\epsilon_g + \Delta = 1.188(6)$ eV.

With $\epsilon_g = 0.888$ (5) eV, and $\delta\epsilon_g = 0.0056$ eV as determined from the observed $(1/R)\Delta R/\Delta S$ structure at the D_1 edge in zero magnetic field (see Sec. IV A), we deduce $\Delta = 0.294$ (5) eV. This value is in excellent agreement with that obtained from the inflection point in the $\Delta R/R$ structure for the D_2 edge at zero magnetic field. This confirms Mavroides's[19] observation that it is the inflection point instead of the minimum in the $\Delta R/R$ structure which corresponds to the transition energy. In the above determination of Δ, the exciton binding energy for the split-off hole and the conduction electron was neglected. If, indeed, the transition between the split-off band and the conduction band involves the creation of a bound exciton, our value of Δ should be increased by 0.0015 eV which is the binding energy of this exciton calculated on the basis of the hydrogenic model. Hence our best value for the spin-orbit splitting energy is $\Delta = 0.296 \pm 0.002$ eV.

The difference of energies for the LCP and RCP transitions corresponding to the same n is also obtained from Eq. (41) as

$$\Delta\mathcal{E}_{so\to c} = \mathcal{E}^L_{so\to c}(n) - \mathcal{E}^R_{so\to c} = \tfrac{1}{2}(g_c + g_{so})s. \quad (43)$$

Therefore, a plot of $\Delta\mathcal{E}_{so\to c}$ versus s should give a straight line with a slope equal to $\frac{1}{2}(g_c + g_{so})$. In Fig. 7 is shown such a plot for our data. The data points show a considerable scatter about the best straight line through the origin. This large scatter is most probably due to the overlap of the split-off-band-to-conduction-band transitions with the transitions

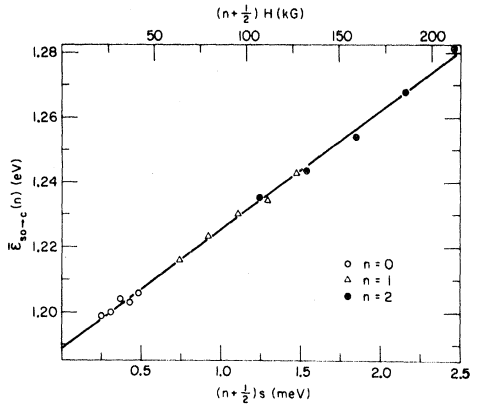

FIG. 6. Plot of the mean energy for the LCP and RCP transitions involving conduction-band levels with the same n as a function of $(n+\frac{1}{2})s$. In the coupled-band scheme, the split-off levels involved in this case have different orbital quantum numbers.

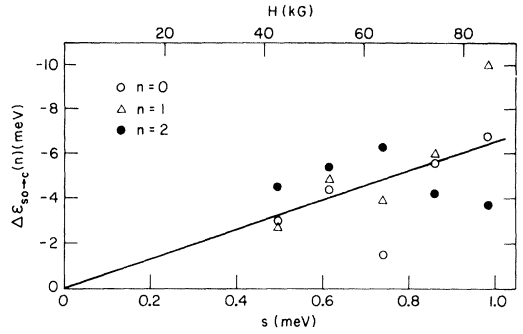

FIG. 7. Plot of the energy difference between the LCP and RCP transitions involving conduction-band levels with the same n as a function of s.

from the light and heavy valence bands to the conduction band. The slope of the line in Fig. 7 gives $g_c + g_{so} = -13.2 \pm 2.8$. According to Eq. (21), g_c is expected to be -3.0 ± 0.2. With this value of g_c, we deduce $g_{so} = -10.2 \pm 3.0$. In view of Eq. (29) our value of -13.2 ± 2.8 for $(g_c + g_{so})$ will give $\kappa^L = 3.3 \pm 0.7$, in good agreement with the determination of $\kappa^L = 3.41 \pm 0.03$ by Hensel and Suzuki.[24]

2. *Light and Heavy Valence-Band-to-Conduction-Band Transitions*

There are a large number of allowed transitions in this category. Many of these transitions cannot be identified in the spectra of Figs. 3 and 4 for the following reasons: (i) The intensity of some of the transitions is so small that they are not observed, and (ii) a number of transitions occur at nearly the same energy so that they are not resolved in our experiment. We can obtain some of the band-edge parameters or some combinations thereof by an analysis of the data for some of the transitions for low quantum numbers.

The first two Landau levels corresponding to $n = -1, 0$ for the a and b sets of the valence band have $M_J = -\frac{1}{2}$ and $M_J = -\frac{3}{2}$, respectively. The eigenvalues of these levels are obtained from Eq. (12) for the a set as

$$\epsilon_a = -s[(\gamma_1^L - \gamma'^L)(n + \tfrac{3}{2}) - \tfrac{1}{2}\kappa^L] + \epsilon_1 . \quad (44)$$

The eigenvalues for the above two levels of the b set are obtained from Eq. (13) as

$$\epsilon_b = -s[(\gamma_1^L + \gamma'^L)(n + \tfrac{3}{2}) - \tfrac{3}{2}\kappa^L] - \epsilon_1 . \quad (45)$$

In each series there is an allowed transition in LCP from the $n = 0$ level of the valence band to the $n = 1$ level of the conduction band. We denote these transitions by a $^+(0)a^c(1)$ and $b^+(0)b^c(1)$. This notation is similar to that used by Pidgeon and Brown[6] except that the numbers in parentheses denote the Landau quantum number n used in the coupled-band scheme instead of the decoupled scheme. If we neglect nonparabolic effects, the above two transitions will occur at energies

$$\mathcal{E}_a = \epsilon_g + \delta\epsilon_g - \epsilon_1 + s[\tfrac{3}{2}(m/m_c) + \tfrac{3}{2}(\gamma_1^L - \gamma'^L) - \tfrac{1}{2}\kappa^L + \tfrac{1}{4}g_c] \quad (46)$$

and

$$\mathcal{E}_b = \epsilon_g + \delta\epsilon_g + \epsilon_1 + s[\tfrac{3}{2}(m/m_c) + \tfrac{3}{2}(\gamma_1^L + \gamma'^L) - \tfrac{3}{2}\kappa^L - \tfrac{1}{4}g_c] . \quad (47)$$

Therefore, the splitting of these transitions will be

$$\Delta\mathcal{E} = \mathcal{E}_b - \mathcal{E}_a = 2\epsilon_1 + s[3\gamma'^L - \kappa^L - \tfrac{1}{2}g_c] . \quad (48)$$

A plot of this splitting versus s is shown in Fig. 8. From the intercept of the straight-line fit to the data points, we get $2\epsilon_1 = -4.6 \pm 0.7$ meV, which represents the strain splitting of the light and heavy valence bands. The negative sign of $2\epsilon_1$ is consistent with the observation of the D_1 edge at an energy higher than ϵ_g. However, the magnitude of $2\epsilon_1$ is somewhat larger than the splitting of the zero-field edge (see Fig. 2). The slope of the line gives $3\gamma'^L - \kappa^L - \frac{1}{2}g_c = 15.6 \pm 1.0$. Using our value of 3.3 ± 0.7 for κ^L determined from the split-off valence-to-conduction-band transitions and $g_c = -3.0 \pm 0.2$, we deduce that

$$\gamma'^L = \tfrac{1}{4}(\gamma_2^L + 3\gamma_3^L) = 5.8 \pm 0.6 .$$

This value of γ'^L is larger than that of 5.33 ± 0.02 obtained with Hensel and Suzuki[25] parameters $\gamma_2^L = 4.30 \pm 0.02$ and $\gamma_3^L = 5.68 \pm 0.02$. This discrepancy is most likely due to incomplete cancellation of exciton effects in taking the difference between $\mathcal{E}_a$ and $\mathcal{E}_b$. When the mean value of $\mathcal{E}_a$ and $\mathcal{E}_b$ is plotted as a function of s as shown in Fig. 8, the

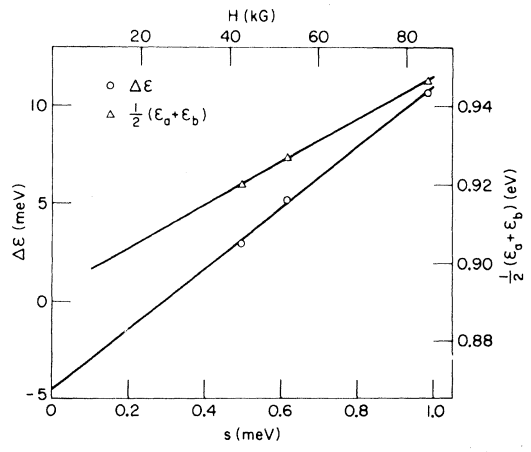

FIG. 8. Plot of the energy difference and the mean energy for the transitions $a^+(0)a^c(1)$ and $b^+(0)b^c(1)$ which involve the $n = 1$ conduction-band levels, and the $n = 0$ (in the coupled-band scheme) light valence-band levels.

slope of the line gives

$$\tfrac{3}{2}[(m/m_c)+\gamma_1^L)]-\kappa^L = 54.8\pm 1.4 \ .$$

With $\kappa^L = 3.3\pm 0.8$ and $m/m_c = 26.3\pm 0.4$, as determined in Sec. IV B 3, we obtain $\gamma_1^L = 12.4\pm 1.9$. This is smaller than the value of 13.38 ± 0.02 given by Hensel and Suzuki.[25] This is more evidence for the presence of exciton effects in these transitions to the $n=1$ levels of the conduction band.

Let us now consider the heavy-band-to-conduction-band transitions between Landau levels with large n. In this case the separation between the consecutive heavy band levels is independent of n for small magnetic fields. This is also true for the high magnetic fields used in our experiment because the nonparabolic effects for the heavy band are negligible for the energy range of interest to us. Therefore, the decrease in the energy separation $\Delta\mathcal{E}(n, n-1)$ between transitions to conduction-band levels n and $n-1$ with increasing n reflects the nonparabolicity of the conduction band. This is shown in Fig. 9 which is a plot of $\Delta\mathcal{E}(n, n-1)/s$ versus ns for the spectra of Figs. 3 and 4 obtained with $H = 84.9$ kG. The solid curve, which is a least-squares fit of the data to a straight line, has a slope of -1.04 ± 0.1 meV^{-1} and an intercept of 29.0 ± 0.6 on the $\Delta\mathcal{E}(n, n-1)/s$ axis. The above value of the intercept is a measure of the reciprocal of the reduced mass ratio for the conduction and heavy valence bands, i.e.,

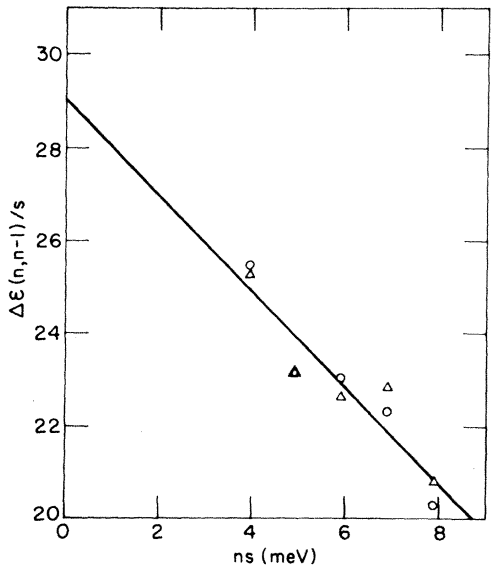

FIG. 9. Plot of $\Delta\mathcal{E}(n, n-1)/s$ versus ns for the heavy-valence-band-to-conduction-band transitions with $n=3$, 4, 5, 6, 7, and 8 observed at a magnetic field of 84.9 kG with RCP and LCP radiation (see Figs. 3 and 4).

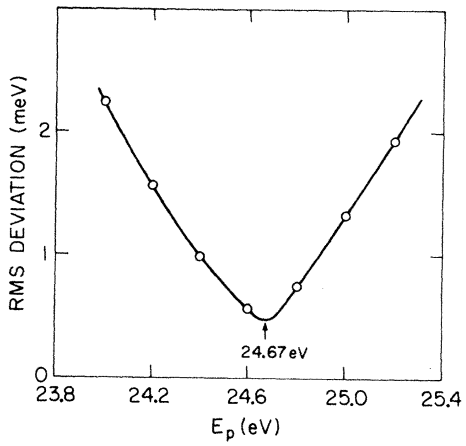

FIG. 10. Root-mean-square deviation of the observed energies for the heavy-valence-band-to-conduction-band transitions from those calculated from Eqs. (12) and (13) with $\gamma_1^L = 13.38$, $\gamma_2^L = 4.30$, $\gamma_3^L = 5.68$, $\kappa^L = 3.41$, and $F=0$. The following 12 transitions were used in the calculation of the rms deviation: $a^-(3)a^c(2)$, $b^-(3)b^c(2)$, $a^-(4)a^c(3)$, $b^-(4)b^c(3)$, $a^-(6)a^c(5)$, $b^-(6)b^c(5)$, $a^-(2)a^c(3)$, $b^-(2)b^c(3)$, $a^-(3)a^c(4)$, $b^-(3)b^c(4)$, $a^-(5)a^c(6)$, and $b^-(5)b^c(6)$ for $H=53.1$ and 84.9 kG.

$$m/m_r = m/m_c - m/m_h = 29.0\pm 0.6 \ .$$

Using Hensel-Suzuki[25] parameters for the valence band, we find that $-m/m_h = 2.96\pm 0.06$ for the [110] direction. With this value for m/m_h, we deduce $m/m_c = 26.0\pm 0.6$ which compares well with the value of 27.1 ± 1 obtained by Roth *et al.*[15] from magnetoabsorption measurements, and the theoretical value of 26.3 corresponding to $m_c = 0.038m$ given by Dresselhaus and Dresselhaus.[26] The slope of the solid curve in Fig. 9 is a determination of the nonparabolicity of the conduction band. Stradling and Wood[27] have given an expression [see Eq. (9) of Ref. 27] for the energy of Landau levels of the nonparabolic conduction band deduced on the assumption that the terms greater than k^4 are negligible. Using this equation, the slope of the curve in Fig. 9 should be

$$-2\left(\frac{m}{m_c}\right)^2 1\left(-\frac{m_c}{m}\right)^2 \frac{3\epsilon_g + 4\Delta + 2\Delta^2/\epsilon_g}{(\epsilon_g+\Delta)(3\epsilon+2\Delta)} \ .$$

With $m/m_c = 26.0$, $\epsilon_g = 0.888$ eV, and $\Delta = 0.296$ eV, the theoretically expected value for the slope is -1.31 meV^{-1}. This indicated that the measured nonparabolicity is somewhat less than that implied in Eq. (9) of Ref. 27.

3. *Use of the* 4×4 *Determinantal Equations* (12) *and* (13) *for Analysis of Experimental Data*

In this analysis we will use the valence-band parameters $\gamma_1^L, \gamma_2^L, \gamma_3^L$, and κ^L as determined by Hensel and Suzuki.[24,25] With $\epsilon_g = 0.888(5)$ eV and

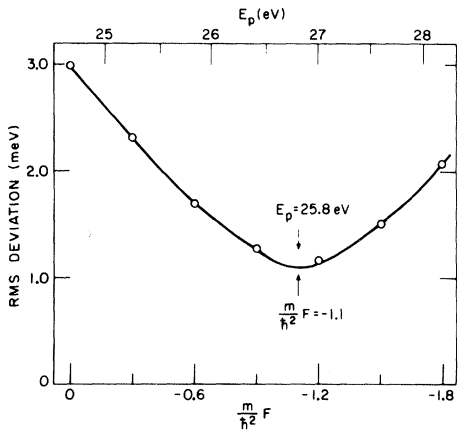

FIG. 11. Root-mean-square deviation of the observed energies for the light-valence-band-to-conduction-band transitions from those calculated using Eqs. (12) and (13) with $\gamma_1^L = 13.38$, $\gamma_2^L = 4.30$, $\gamma_3^L = 5.68$, $\kappa^L = 3.41$, and $m_c = 0.038m$. The following ten transitions were used in calculating the rms deviation: $a^+(3)a^c(2)$, $a^+(4)a^c(3)$, $a^+(5)a^c(4)$, $a^+(6)a^c(5)$, $a^+(7)a^c(6)$, $b^+(1)b^c(2)$, $b^+(2)b^c(3)$, $b^+(3)b^c(4)$, $b^+(4)b^c(5)$, $b^+(5)b^c(6)$ for $H = 53.1$ and 84.9 kG.

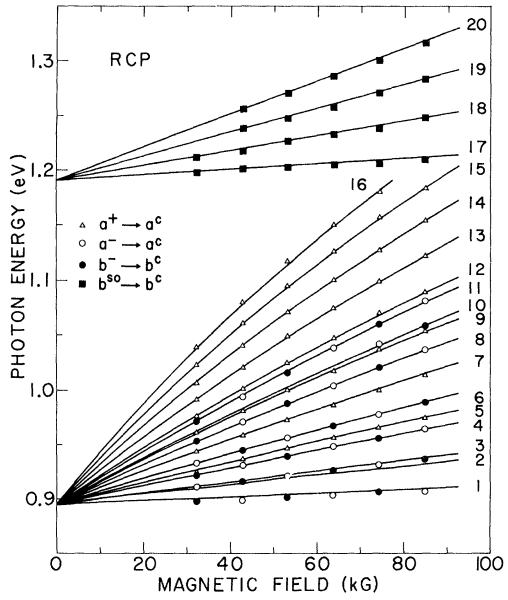

FIG. 12. Plot of the photon energy versus magnetic field for a number of transitions allowed in the Faraday configuration with RCP radiation. The solid lines are the theoretical curves obtained from Eqs. (12) and (13) with the same parameters as for Fig. 3. The numbers next to each curve denote the following transitions: (1) $a^-(1)a^c(0)$, $b^{-1}b^c(0)$; (2) $a^+(1)a^c(0)$; (3) $a^-(2)a^c(1)$, $b^-(2)b^c(1)$; (4) $a^-(3)a^c(2)$, $b^-(3)b^c(2)$; (5) $a^+(2)a^c(1)$; (6) $a^-(4)a^c(3)$, $b^-(4)b^c(3)$; (7) $a^+(3)a^c(2)$; (8) $a^-(6)a^c(5)$, $b^-(6)b^c(5)$; (9) $a^+ \times (4)a^c(3)$; (10) $a^-(7)a^c(6)$, $b^-(7)b^c(6)$; (11) $a^-(8)a^c(7)$, $b^-(8) \times b^c(7)$; (12) $a^+(5)a^c(4)$; (13) $a^+(6)a^c(5)$; (14) $a^+(7)a^c(6)$; (15) $a^+(8)a^c(7)$; (16) $a^+(9)a^c(8)$; (17) $b^{so}(1)b^c(0)$; (18) $b^{so}(2)b^c(1)$; (19) $b^{so}(3)b^c(2)$; (20) $b^{so}(4)b^c(3)$.

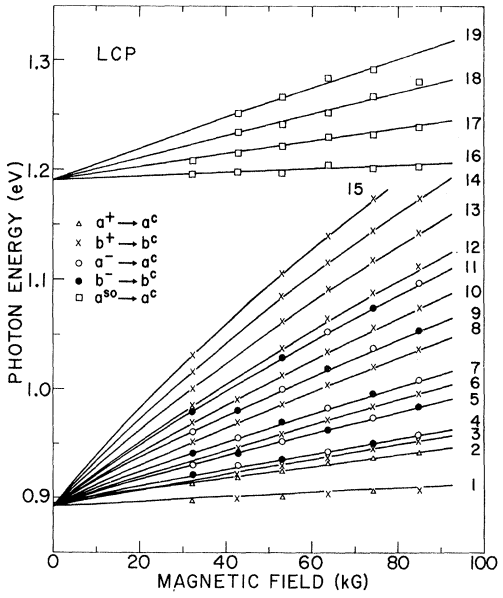

FIG. 13. Plot of the photon energy versus magnetic field for a number of transitions allowed in the Faraday configuration with LCP radiation. The solid lines are the theoretical curves obtained from Eqs. (12) and (13) with the same parameters as for Fig. 3. The numbers next to each curve denote the following transitions: (1) $b^+(-1)b^c(0)$; (2) $a^+(0)a^c(1)$; (3) $b^+(0)b^c(1)$; (4) $a^-(1)a^c(2)$, $b^-(1)b^c(2)$; (5) $a^-(2)a^c(3)$, $b^-(2)b^c(3)$; (6) $b^+(1)b^c(2)$; (7) $a^-(3)a^c(4)$, $b^-(3)b^c(4)$; (8) $b^+(2)b^c(3)$; (9) $a^-(5)a^c(6)$, $b^-(5) \times b^c(6)$; (10) $b^+(3)b^c(4)$; (11) $a^-(7)a^c(8)$, $b^-(7)b^c(8)$: (12) $b^+ \times (4)b^c(5)$; (13) $b^+(5)b^c(6)$; (14) $b^+(6)b^c(7)$; (15) $b^+(7)b^c(8)$; (16) $a^{so}(-1)a^c(0)$; (17) $a^{so}(0)a^c(1)$; (18) $a^{so}(1)a^c(2)$; (19) $a^{so}(2)a^c(3)$.

$\Delta = 0.296$ eV as deduced from the analysis of the zero-field piezoreflectance spectrum and the magnetopiezoreflectance due to the split-off valence-to-conduction-band transitions, we calculate the energies for the allowed heavy-valence-to-conduction-band transitions for many values of the parameter E_p with $F = 0$. The root-mean-square deviation of the calculated energies from the experimental values for a number of transitions observed at $H = 53.1$ and 84.9 kG is shown in Fig. 10. The minimum in the root-mean-square deviation occurs at $E_p = 24.67$ eV. But this value of E_p along with $F = 0$ does not provide an equally good agreement for the light-valence-to-conduction-band transitions. However, if we choose a small but negative value for F and at the same time increase E_p in such a manner that the conduction-band-edge mass as given by Eq. (20) remains unchanged, the agreement between experimental and calculated values improves. This behavior is shown in Fig. 11 which is a plot of the root-mean-square deviation for a number of the light-valence-to-conduction-band transitions ob-

TABLE I. Effective masses and g factors for the conduction and split-off bands at k = 0.

	MPR (~30 °K)	Magnetoabsorption	MPR (Ref. 5) (300 °K)	Theory (Ref. 26) (300 °K)
m_c	$(0.038 \pm 0.005)m$	$0.038m$(300 °K) (Ref. 18) $(0.0.37 \pm 0.0013)m$(4.2 °K)[a] $0.037m$(77 °K) (Ref. 28)	$(0.042 \pm 0.005)m$	$0.038m$
g_c	-3.0 ± 0.2	-2.5(4.2 °K)[a] -2.0(5 °K) (Ref. 29)	...	...
m_{so}	$(-0.095 \pm 0.007)m$	...	$(-0.084 \pm 0.025)m$	$-0.10m$
g_{so}	-10 ± 3	...		

[a]Reference 15. Since a cold-finger Dewar was used in the measurements, the sample temperature was presumably higher than 4.2 °K which represents the temperature of liquid-helium coolant.

served at $H = 53.1$ and 84.9 kG. In this manner we find that $F = (-1.1 \pm 0.2)\hbar^2/m$ and $E_p = 26.8 \pm 0.4$ eV provide the best fit for the experimental data. The variation in the photon energy as a function of the magnetic field is shown in Figs. 12 and 13 for a number of transitions observed with RCP and LCP radiation. Except for the split-off valence-to-conduction-band transitions, and a small deviation for the low quantum transitions, presumably due to exciton effects neglected in our analysis, the experimental data are in excellent agreement with the computed results shown by the solid curves. With the band parameters used in our computations, the following values for the band-edge masses and g factors are obtained from Eqs. (20), (21), (34), and (35): $m_c = (0.0380 \pm 0.0005)m$, $g_c = 3.0 \pm 0.2$, $m_l = -0.042m$, and $m_h = -0.34m$. With these values of m_c and g_c, we deduce from our results for the split-off valence-to-conduction-band transitions, $m_{so} = -(0.095 \pm 0.007)m$ and $g_{so} = -10 \pm 3$.

Finally we show in Table I [28,29] a comparison of our values for the effective masses and g factors of the conduction and split-off bands with those obtained by others.

V. CONCLUSIONS

We believe that this is the first careful application of the stress-modulation technique for the accurate determination of the band-edge parameters for the conduction and valence bands in germanium. This work also demonstrates that the inherent bias against magnetoabsorption experiments with stressed samples is not well founded especially when the presence of stress is taken into account in the analysis of the data as in the present case.

ACKNOWLEDGMENTS

The author would like to thank Professor Benjamin Lax for stimulating interest in this investigation; Dr. S. H. Groves, Dr. C. R. Pidgeon, and M. Reine for many useful discussions concerning the analysis of the data; and T. R. Hart for a critical reading of the manuscript. The assistance of L. V. Sousa with experiments is greatly appreciated.

*Supported by the U. S. Air Force Office of Scientific Research.

[1]S. Zwerdling, B. Lax, L. M. Roth, and K. J. Button, Phys. Rev. 114, 80 (1959).

[2]Q. H. F. Vrehen and B. Lax, Phys. Rev. Letters 12, 471 (1964).

[3]W. E. Engeler, H. Fritzsche, M. Garfinkel, and J. J. Tiemann, Phys. Rev. Letters 14, 1069 (1965).

[4]R. L. Aggarwal, L. Rubin, and B. Lax, Phys. Rev. Letters 17, 8 (1966); J. G. Mavroides, M. S. Dresselhaus, R. L. Aggarwal, and G. F. Dresselhaus, J. Phys. Soc. Japan Suppl. 21, 184 (1966).

[5]S. H. Groves, C. R. Pidgeon, and J. Feinleib, Phys. Rev. Letters 17, 643 (1966).

[6]C. R. Pidgeon and R. N. Brown, Phys. Rev. 146, 575 (1966).

[7]The magnitude of the static strain is not very reproducible. Variations of the order of 50% have been observed between runs made under similar conditions.

[8]Polaroid Corporation, Cambridge, Mass. 02139.

[9]W. H. Kleiner and L. M. Roth, Phys. Rev. Letters 2, 334 (1959).

[10]F. H. Pollak and M. Cardona, Phys. Rev. 172, 816 (1968).

[11]H. Hasegawa, Phys. Rev. 129, 1029 (1963).

[12]S. H. Groves has pointed out that certain small constant terms were omitted from the split-off band elements in Eqs. (17) and (18) of Ref. 6 (private communication).

[13]H. Ehrenreich, J. Appl. Phys. Suppl. 32, 2155 (1961).

[14]E. O. Kane, J. Phys. Chem. Solids 1, 249 (1957).

[15]L. M. Roth, B. Lax, and S. Zwerdling, Phys. Rev. 114, 90 (1959).

[16]J. M. Luttinger, Phys. Rev. 102, 1030 (1956).

[17]V. Evtuhov, Phys. Rev. 125, 1869 (1962).

[18]E. Burstein, G. C. Picus, R. F. Wallis, and F. Blatt, Phys. Rev. 113, 15 (1959).

[19]J. G. Mavroides, in *Physics of Solids in Intense Magnetic Fields*, edited by E. D. Haidemenakis (Plenum, New York, 1969), p. 206.
[20]W. Paul and D. M. Warschauer, in *Solids Under Pressure*, edited by W. Paul and D. M. Warschauer (McGraw-Hill, New York, 1963), p. 226.
[21]G. G. Macfarlane, T. P. McLean, J. E. Quarrington, and V. Roberts, Proc. Phys. Soc. (London) 71, 863 (1958).
[22]M. V. Hobden, J. Phys. Chem. Solids 23, 821 (1962).
[23]B. O. Seraphin, Phys. Rev. Letters 14, 138 (1965).
[24]J. C. Hensel and K. Suzuki, Phys. Rev. Letters 22, 838 (1969).
[25]J. C. Hensel and K. Suzuki, Phys. Rev. Letters 21, 983 (1968).
[26]G. Dresselhaus and M. S. Dresselhaus, Phys. Rev. 160, 649 (1967).
[27]R. A. Stradling and R. A. Wood, J. Phys. C 1, 1711 (1968).
[28]Q. H. F. Vrehen, Phys. Rev. 145, 675 (1966).
[29]E. J. Johnson, in *Proceedings of the International Conference on the Physics of Semiconductors, Moscow*, 1968 (Nauka, Leningrad, 1968), Vol. 1, p. 276.

PHYSICAL REVIEW B VOLUME 2, NUMBER 2 15 JULY 1970

Split-Off Valence-Band Parameters for GaAs from Stress-Modulated Magnetoreflectivity

M. Reine,*†‡ R. L. Aggarwal, and B. Lax†

Francis Bitter National Magnet Laboratory, § *Massachusetts Institute of Technology, Cambridge, Massachusetts* 01239

and

C. M. Wolfe

Lincoln Laboratory, ‖ *Massachusetts Institute of Technology, Lexington, Massachusetts* 02173

(Received 17 September 1969)

We have measured the spin-orbit split-off valence-band parameters in high-purity epitaxial GaAs at ~30 °K by means of stress-modulated interband magnetoreflectivity. Our results are $(m/m_c - m/m_{so}) = 21.5 \pm 0.4$, $g_c + g_{so} = -4.7 \pm 1.0$, where m_c and m_{so} are the conduction-band and split-off-band effective masses and g_c and g_{so} are the corresponding effective g factors. From these results, we deduce $m_{so}/m = -0.154 \pm 0.010$, $g_{so} = -4.9 \pm 1.0$, and $\kappa^L = 1.2 \pm 0.25$, where κ^L is related to the antisymmetric constant introduced by Luttinger.

I. INTRODUCTION

At the center of the Brillouin zone, the spin-orbit split-off valence band in GaAs lies at an energy $\Delta \approx 0.34$ eV below the degenerate light- and heavy-hole bands. Optical transitions from this band to the conduction band have previously been observed in both absorption[1] and electroreflectance.[2] In this paper, we present the first experimental results of magneto-optical effects associated with this transition. From our data, we are able to determine the first experimental values for the effective mass and the effective g factor for the split-off band. We used the differential technique of stress modulation[3,4] together with samples of epitaxially grown n-type GaAs prepared by Lincoln Laboratory. Stress-modulated or electric-field-modulated magnetoreflectivity has previously provided data on the split-off bands in Ge,[5,6] InSb,[7] InAs,[8] and GaSb.[9] The extension of this type of experiment to GaAs, however, was not possible until the epitaxial process made available material of exceptional purity.

The first estimate of Δ, the spin-orbit splitting, for GaAs was made by Braunstein[10] from intervalence-band-absorption measurements in p-type material. He found $\Delta \approx 0.33$ eV; using this together with Kane's expressions,[11] he estimated the ratios of the split-off-band effective mass to those of the light- and heavy-hole bands. In the same way, Ehrenrich[12] deduced the value $m_{so} \approx -0.2m$ for the split-off-band effective mass. Sturge[1] measured the absorption edge for transitions from the split-off band to the conduction band and found $\Delta = 0.35 \pm 0.01$ eV. Seraphin[2] studied this transition with the electroreflectance technique as a function of temperature from 200 °K to 375 °K. He determined $\Delta = 0.348 \pm 0.002$ eV and showed that the temperature dependence of Δ was negligible compared to that of the energy gap. In later electroreflectance experiments on GaAs -